Near-Wall Study of a Turbulent Boundary Layer Using High-Speed Tomo-PIV

Fabio J.W.A. Martins, Jean-Marc Foucaut, Luis F.A. Azevedo and Michel Stanislas

Abstract The fundamental study of the near-wall structure organization in turbulent flows is crucial to understand the self-generation process of turbulence. To investigate such phenomena, an experiment of high-repetition, 6-camera tomo-PIV in a boundary layer was performed. Vector fields generated from BIMART high-quality reconstructed volumes resulted in low measurement uncertainties. The comparison of turbulence statistics from tomographic PIV and hot-wire anemometer data shows an excellent agreement. Preliminary vortex detection from Q-criterion is presented and allows the identification of dispersed vortices around the low-speed streaks in the boundary layer. Nevertheless an accurate identification of turbulent structures is not yet achieved. The postprocessing is being reviewed and the discussion of the interaction and evolution of turbulent structures will be addressed in a future paper.

1 Introduction

The turbulence structure near the wall in a boundary layer has challenged researchers over the last six decades due to its importance as a driver in innumerous practical engineering applications. In this turbulent flow, kinetic energy from the free flow is converted into turbulent fluctuations and then dissipated into internal energy by the viscosity. A population of many eddies of different scales interact with each other in a complex phenomenon of a continuous self-sustaining process. The presence of quasi-periodic patterns of coherent motion in the flow seems to be responsible for the maintenance of turbulence in a boundary layer [1, 5, 23, 27]. Nonetheless, the near-wall turbulence structures, their evolution, and their interplay are still not fully understood [9, 28].

F.J.W.A. Martins · J.-M. Foucaut · M. Stanislas (✉)
Laboratoire de Mécanique de Lille (LML), Villeneuve-d'Ascq, France
e-mail: michel.stanislas@ec-lille.fr

L.F.A. Azevedo
Mechanical Engineering Department, PUC-Rio, Rio de Janeiro, Brazil

Turbulence measurements achieved a notorious improvement with the recent advances in Particle Image Velocimery (PIV). Nowadays, variations of this nonintrusive technique are able to capture the full three-dimensionality of unsteady flows by means of multi-plane PIV [15], three-dimensional particle tracking velocimetry (3D PTV) [16], defocusing PIV [21], holographic and digital holographic PIV (HPIV and DHPIV) [26], scanning-PIV [13], and tomo-PIV [8]. This work explores the latter, which has a high potential of 3D-3C velocity measurement [24].

The tomographic PIV approach is based on the reconstruction of the particle distribution inside an illuminated volume of a seeded flow. The light scattered by the particles is recorded by multiple, simultaneous camera views, from which the images are used to reconstruct the volume. The instantaneous flow is estimated by the particle displacement between two light pulses, through a 3D cross-correlation over a pair of reconstructed volumes calculated from these views [8]. The reconstruction of the particles from a limited number of views is an indeterminated system solved by algebraic techniques, which are very time consuming [2, 29, 33]. Fortunately, alternative methods for optimizing the reconstruction process were created in order to improve the quality and to decrease the computational time [7, 20, 22, 33].

Recently, Thomas and co-workers [29] proposed the block-iterative multiplicative algebraic reconstruction technique (BIMART) [4], which, in their synthetic data, obtained an equivalent accuracy as the classic MART [8] spending half of its processing time.

In the present study, a 6-camera high-repetition tomo-PIV was used to study the unsteady character of the near-wall boundary layer flow over a flat plate using a spanwise-wall-normal thin volume. The final purpose of the work is to access the full velocity gradient tensor and to reconstruct the time history of the turbulent structures.

2 Experimental Setup

The turbulent boundary layer tomo-PIV experiment took place in the Laboratoire de Mécanique de Lille (LML) large-sized wind tunnel, whose boundary layer can reach up to 300 mm thickness for a Reynolds number based on the momentum thickness, R_θ, of 8000. The tunnel test section is 1 m high, 2 m wide and 20 m long to allow for the development of the boundary layer [5]. The closed-loop wind tunnel is able to maintain the air temperature to within ± 0.2 K and presents a free streamwise velocity stabilization of ± 0.5 %.

The tomographic PIV arrangement was composed of six high-speed CMOS cameras: three Phantom V9, one Phantom V10, and two Photron Fastcam APX [11]. All of them recorded a spanwise-wall-normal volume produced by a Quantronix laser (2×30 mJ@1kHz) as can be seen in Fig. 1. The cameras 1–6 were mounted on Scheimpflug adapters positioned under the wind tunnel in a forward scattering configuration with θ_z angles of about $-35°$, $-145°$, $-145°$, $-35°$, $-135°$ and $-45°$, subsequently, and θ_y of $35°$, $145°$, $-145°$, $-35°$, $180°$ and $0°$ as depicted in Fig. 2. The Phantom cameras (1600×1200 pixels@1kHz and pixel size of 11.5 μm)
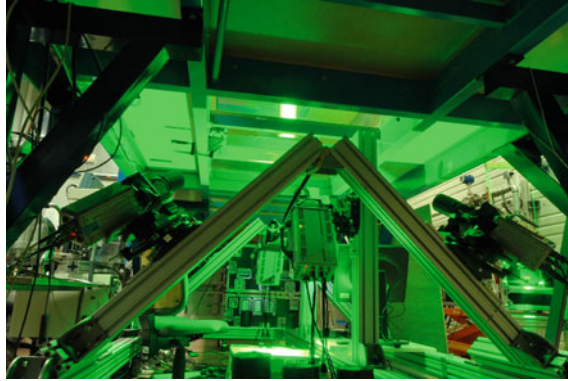
Fig. 1 Cameras imaging an illuminated volume (upper-center position in the picture) assembled in a tomo-PIV arrangement under the wind tunnel
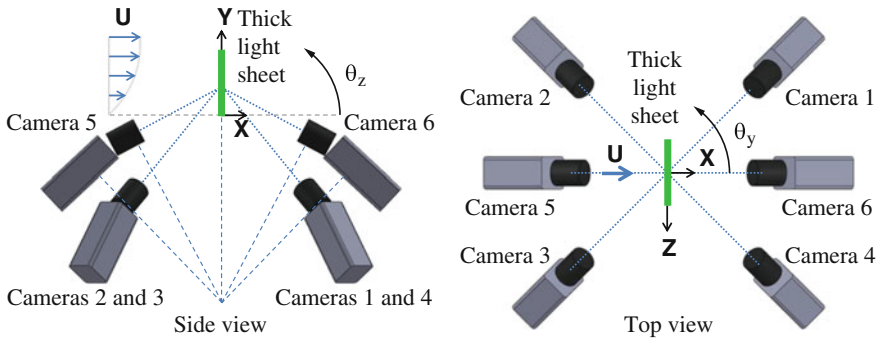

Fig. 2 Sketch of the cameras arrangement in the boundary layer experimental setup

were equipped with micro Nikkor 200 mm lenses at f# 5.6, while the Photron cameras (1024 × 1024 pixels@2kHz and pixel size of 17 μm) were equipped with micro Nikkor 105 mm lens at f# 5.6 combined with a doubler. The laser volume thickness was carefully limited to 5 mm by a knife-edge filter to create an investigation volume of $5 \times 45 \times 45$ mm^3 (i.e. $40 \times 360 \times 360$ wall units). This thin-volume was chosen in order to overcome some difficulties with low light energy [24] and to improve the measurement accuracy [3].

The whole flow was seeded with polyethylene glycol smoke, which generates particles with sizes of about 1 μm. The PIV images were recorded at 1 kHz with a time delay between pulses of 300 μs. The maximum gray level, not including reflections at the wall, was 155 in 8-bit images and the particle-image size was about 1 to 2 pixels. A total of 5 runs of 1725 tomo-PIV fields from an average particle per pixel of 0.05 ppp were recorded.

The cameras were calibrated using a pinhole model [32]. The calibration target was transparent in order to allow the visualization of the markers from both sides.

It was made by printing a crosses pattern on a transparent plastic sheet, which was sandwiched between two 2 mm-thick glass plates. The yz-target plane was scanned in seven equally spaced, out-of-plane positions from $x = -3$ to $x = 3$ mm. A micrometer with $5\,\mu$m precision was used as a translation stage. The crosses pattern presented a distance of 5 mm between two consecutive markers in both y and z directions.

Due to the form that the target was manufactured, the refraction through the 2 mm-thick glass plates created significant triangulation errors. After the removal of the target, the error between the position of the markers along x from the cameras placed downstream and the ones upstream were greater than 2 mm. So, a large number of spurious particle matchings appeared and spread the disparity peak, making the correction of the mapping function by the standard self-calibration method [31] very difficult. To circumvent this problem, the target planes along x were artificially translated by 1.1 mm for the downstream cameras and -1.1 mm for the upstream ones. These values were computed taking into account the refraction properties. An initial self-calibration was applied using the pinhole model with a longitudinal translation on low particle density images followed by three more self-calibration steps for each experimental run. The final pinhole mapping functions had projection errors of about 0.01 pixel and maximum triangulation errors lower than 0.18 pixel, which is enough to produce good quality reconstruction volumes [8, 31]. It is noteworthy that this problem is not faced in the stereoscopic PIV [9].

3 Volume Reconstruction and PIV Processing

The reconstruction was performed using the BIMART [29], given by the equation

$$
E(x_j, y_j, z_j)^{n+1} = E(x_j, y_j, z_j)^n \prod_{i,k \in B_Q \cap N_j} \left(\frac{I_k(x_i, y_i)}{\sum_{l \in L_{i,k}} w_{i,l,k} E(x_l, y_l, z_l)^n} \right)^{\mu w_{i,j,k}},
$$

(1)

where $I(x, y)$ are the image pixel intensity distribution, $E(x, y, z)$ are the voxel intensity distribution inside the reconstructed volume, $L_{i,k}$ represents the voxels intercepted by the line of sight (LOS) of the ith pixel in the kth camera, $w_{i,j,k}$ is a weight function related to the contribution of the jth voxel (x_j, y_j, z_j) in these pixels, N_j represents the pixels that have a LOS crossing a given voxel j, B_Q contains the pixels inside the block Q, n indicates the iteration and μ is a relaxation parameter.

In order to improve the volume reconstruction quality and to reduce the time requirements, a meticulous analysis was performed. The optimization of the tomo-PIV parameters together with several image preprocessing methods were studied on synthetic and experimental data [17, 29]. As a result, a conservative 8-iteration BIMART with a block size equal to four, with an initialization based on the min-

imum line of sight (MinLOS) [18] and with 2-iteration volume filter of 0.004 was applied to reconstruct the volumes with a voxel size of $71 \, \mu m$. The 6-camera images were preprocessed using a time-average background subtraction followed by a 3×3 Gaussian filtering before the reconstruction procedure [17].

From a pair of volumes comprising the particle distribution, the velocity fields were computed by means of a 3D multipass cross-correlation with subpixel shift. Two initial steps with an interrogation window size of $36 \times 72 \times 72$ voxels were performed followed by three final steps with a window size of $36 \times 36 \times 36$ voxels and 75 % overlap. The resulting 8625 vector fields of $5 \times 67 \times 67$ grid were validated by a normalized median filtering [30] and the spurious vectors, amounting to about 1.5 %, were successfully replaced by the interpolation of their adjacent neighbors.

The tomo-PIV software was developed in C^{++} as a result of the partnership between Pprime (Poitiers), Coria (Rouen), and LML (Lille) laboratories. The post-processing is based on the Matlab platform.

4 Results and Discussion

The comparison of the velocity statistics of tomographic PIV against the standard hot-wire anemometer data (HWA) [5] are presented in the Fig. 3. From Fig. 3a, b, it can be verified that the tomo-PIV and HWA velocity profiles virtually collapse and that they perfectly follow the theoretical curves. Figure 3c shows an excellent agreement between the turbulent–velocity fluctuation profiles from tomo-PIV and HWA. However, the tomo-PIV data is slightly under the HWA curve, which insinuates that the size of interrogation window is filtering the data. A small difference is observed at points near the wall where the reflections of the laser light were stronger. It is also important to mention that the $\sqrt{<v'^2>}/u_{\tau_w}$ near the wall for the hot-wire anemometer is overestimated due to the size of the probe. From Fig. 3d, a perfect concordance with the Van Driest model is observed. Finally, the agreement between the tomo-PIV and HWA is an indication that the record time of 8.62 s is sufficient to reach converged statistics.

Figure 4 compares the probability densities of the three velocity components calculated at 50 wall units by tomo-PIV and HWA. A small discrepancy is observed for $v'/\sqrt{<v'^2>}$ and $w'/\sqrt{<w'^2>}$ measured by the two techniques probably due to a slight difference in the HWA and tomo-PIV experimental conditions as the data were collected at distinct moments. In Fig. 4c, a marginal asymmetry is observed in the tomo-PIV that is seemingly caused by a little reminiscence of the peak-locking effect, since the deformation method was not applied to the interrogation window during the correlation process [24].

From the 3C-3D velocity field, the velocity gradients in x, y and z directions were computed by a second-order central difference scheme [10] to access both the velocity gradient tensor and the divergence of the fluctuating velocity.
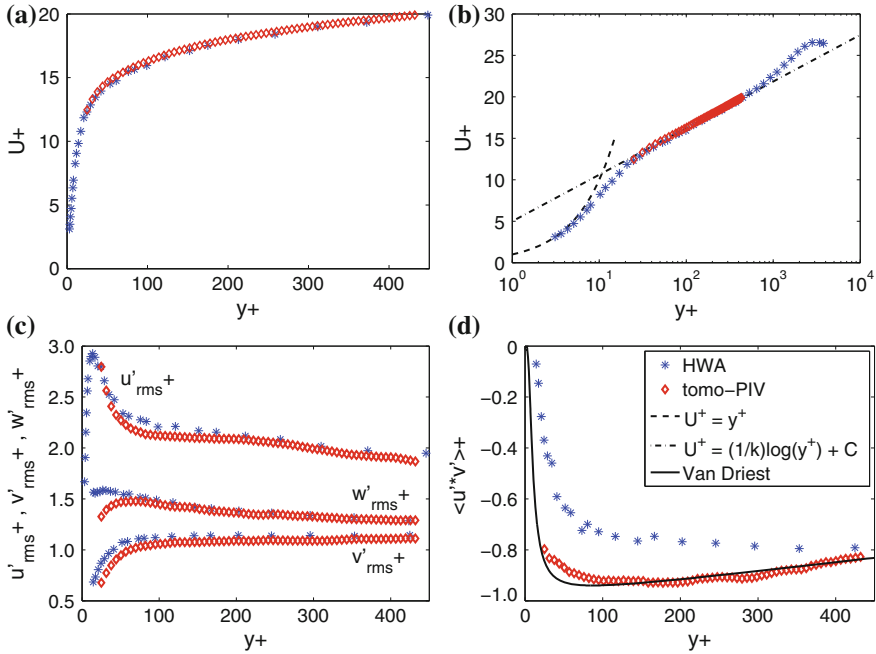
Fig. 3 Streamwise velocity profile in **a** linear and **b** semi-log scales and turbulent velocity fluctuations **c** $\sqrt{<u'^2>}/u_{\tau_w}$, $\sqrt{<v'^2>}/u_{\tau_w}$ and $\sqrt{<w'^2>}/u_{\tau_w}$ and **d** $\sqrt{<u'v'>}/u_{\tau_w}$
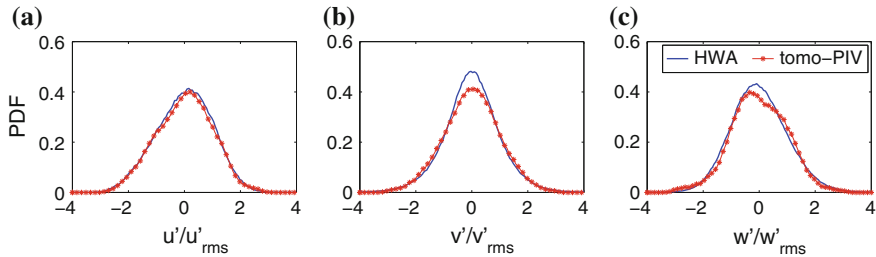
Fig. 4 Probability density functions at $y^+ = 50$ for **a** $u'/\sqrt{<u'^2>}$, **b** $v'/\sqrt{<v'^2>}$ and **c** $w'/\sqrt{<w'^2>}$

The analysis of the local velocity-fluctuation divergence allows us to estimate the uncertainty on the velocity field [3, 19]. Since, for an incompressible flow without error measurements, the divergence of the velocity must be zero, the uncertainty in the gradient $\delta(\partial u'_i/\partial x_i)$ can be computed as the root-mean-square of the divergence. Assuming that the vector spacing and the uncertainty $\delta(u)$ in each direction are uniform, the uncertainty on the velocity can be given as

$$\delta(u) = \sqrt{\frac{2\Delta^2}{3}} \delta\left(\frac{\partial u'_i}{\partial x_i}\right), \tag{2}$$
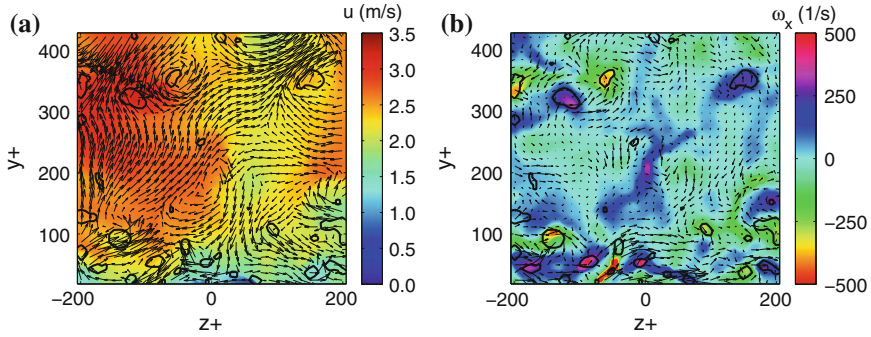
Fig. 5 Comparison between an instantaneous **a** velocity field and its correspondent **b** vorticity. The color represent the third component and the black isolines are the Q-criterion for both plots

where Δ is the physical spacing between velocity vectors, in this work equal to 635 μm (i.e. 6.5 wall units).

The root-mean-square of the divergence through the volume was $49.3\,\mathrm{s}^{-1}$, which corresponds to a velocity uncertainty of 0.0256 m/s (equivalent to 0.12 voxels). This good value for a tomo-PIV air experiment was probably achieved due to the measurement in a thin volume and the use of six cameras. The uncertainty level obtained is comparable to the literature [3, 25].

Preliminary results for the detection of turbulent structures are presented in Fig. 5. The middle plane of an instantaneous 3D-velocity field from tomographic PIV is plotted together with the corresponding 3D-vorticity field. The vortical detection was made by the Q-criterion, whose isolines are embedded in the plots. To enhance the visualization, only one over two vectors are displayed. As can be seen in the Fig. 5b, the isolines appear in the expected regions of high vorticity magnitude.

The Q-criterion [14] identifies vortices as flow regions with positive second invariant of the velocity gradient tensor, i.e., Q > 0, with the requirement of pressure in the eddy region to be lower than the ambient pressure. In this work, the additional pressure condition was not used as it is done by other researchers [6]. The Q-criterion for an incompressible flow is defined as

$$Q = -\frac{1}{2}\frac{\partial u_i}{\partial x_j}\frac{\partial u_j}{\partial x_i}. \tag{3}$$

Since the tomo-PIV data from the present experiment are time resolved, 3D plots, with the third dimension being time, complement the 2D analysis, helping in the inference of turbulent structure dynamics and evolution. In favor of the vortical-structure clarification, the elimination of noise in the vortex detection was made by a robust discrete-cosine-transform filter [12] followed by a volume filtering in the labelized field. The visualization of low-speed streaks together with vortical structures, before and after filtering, are displayed in the Fig. 6. From the sample results presented from this ongoing work, it is possible to identify vortices neighboring the
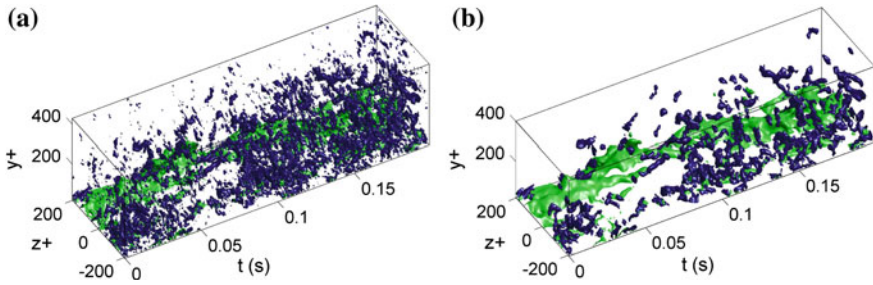
Fig. 6 Interaction between low-speed streaks (in *green*) and turbulent vortical structures (in *blue*) inside a turbulent boundary layer from **a** raw and **b** filtered data

low-speed streaks. The results, however, still do not present sufficient resolution to allow the distinction of boundary layer turbulence structures.

The preliminary results exposed in the present paper clearly indicate the potential of the experiment to allow a comprehensive analysis of boundary layer turbulence structures.

5 Conclusions

A tomo-PIV technique with six high-speed cameras was applied to study the unsteady character of the near-wall flow in a wind tunnel boundary layer for a momentum-thickness Reynolds number of 8000.

The cameras were carefully calibrated using a pinhole model and a modified self-calibration procedure. Due to refraction in the target, a procedure of artificial translation of target planes was necessary to minimize the errors.

The optimization of the image preprocessing and the volume reconstruction was successfully performed. The vector fields generated from BIMART reconstructed volumes resulted in low measurement errors, which were estimated by the velocity-fluctuation divergence.

Turbulence statistics from over 8600 vector fields were presented. An excellent agreement between tomographic PIV and hot-wire anemometer data is observed in terms of velocity profiles and turbulent fluctuations. Also, the experimental data match theoretical curves, which reveals that the recording time was sufficient to obtain converged statistics.

The probability density functions of the velocity fluctuations from the tomo-PIV method were also compared against the hot-wire anemometer showing good agreement.

Preliminary vortex detection results were demonstrated in terms of vorticity and Q-criterion, which allow the identification of some vortices interacting with low-speed streaks in the wall boundary layer. Nevertheless, an accurate identification of turbulent structures was not yet achieved and is an ongoing work.

References

1. R. Adrian, C. Meinhart, C. Tomkins, Vortex organization in the outer region of the turbulent boundary layer. J. Fluid Mech. **422**, 1–54 (2000)
2. C. Atkinson, J. Soria, An efficient simultaneous reconstruction technique for tomographic particle image velocimetry. Exp. Fluids **47**(4–5), 553–568 (2009)
3. C. Atkinson, S. Coudert, J.-M. Foucaut, M. Stanislas, J. Soria, The accuracy of tomographic particle image velocimetry for measurements of a turbulent boundary layer. Exp. Fluids **50**(4), 1031–1056 (2011)
4. C. Byrne, Block-iterative algorithms. Int. Trans. Oper. Res. **16**(4), 427–463 (2009)
5. J. Carlier, M. Stanislas, Experimental study of eddy structures in a turbulent boundary layer using particle image velocimetry. J. Fluid Mech. **535**(36), 143–188 (2005)
6. P. Chakraborty, S. Balachandar, R. Adrian, On the relationships between local vortex identification schemes. J. Fluid Mech. **535**(2005), 189–214 (2005)
7. S. Discetti, T. Astarita, A fast multi-resolution approach to tomographic PIV. Exp. Fluids **52**(3), 765–777 (2012)
8. G. Elsinga, F. Scarano, B. Wieneke, B.W. van Oudheusden, Tomographic particle image velocimetry. Exp. Fluids **41**(6), 933–947 (2006)
9. J.-M. Foucaut, S. Coudert, M. Stanislas, J. Delville, Full 3D correlation tensor computed from double field stereoscopic PIV in a high Reynolds number turbulent boundary layer. Exp. Fluids **50**(4), 839–846 (2011)
10. J.-M. Foucaut, M. Stanislas, Some considerations on the accuracy and frequency response of some derivative filters applied to PIV vector fields. Meas. Sci. Technol. **13**(7), 1058–1071 (2002)
11. J.-M. Foucaut, S. Coudert, A. Avelar, B. Lecordier, G. Godard, C. Gobin, L. Thomas, P. Braud, L. David, Experiment of high repetition tomographic PIV in a high Reynolds number turbulent boundary layer wind tunnel, in *PIV'11—Ninth International Symposium on Particle Image Velocimetry*. Kobe, Japan (2011)
12. D. Garcia, Robust smoothing of gridded data in one and higher dimensions with missing values. Comput. Stat. Data Anal. **54**(4), 1167–1178 (2010)
13. T. Hori, J. Sakakibara, High-speed scanning stereoscopic PIV for 3D vorticity measurement in liquids. Meas. Sci. Technol. **15**(6), 1067 (2004)
14. J. Hunt, A. Wray, P. Moin, Eddies, streams, and convergence zones in turbulent flows, in *Studying Turbulence Using Numerical Simulation Databases*, vols. 1, 2, (1988), pp. 193–208
15. C.J. Kähler, J. Kompenhans, Fundamentals of multiple plane stereo particle image velocimetry. Exp. Fluids **29**(1), S070–S077 (2000)
16. H.G. Maas, A. Gruen, D. Papantoniou, Particle tracking velocimetry in three-dimensional flows. Exp. Fluids **15**(2), 133–146 (1993)
17. F. Martins, J.-M. Foucaut, L. Thomas, L. Azevedo, M. Stanislas, Volume reconstruction optimization for tomo-PIV experimental data, in *Final International Workshop on Advanced Flow Diagnostics for Aeronautical Research—AFDAR*, Lille, France (2014)

18. D. Michaelis, M. Novara, F. Scarano, B. Wieneke, Comparison of volume reconstruction techniques at different particle densities, in *15th International Symposium on Applications of Laser Techniques to Fluid Mechanics*. Lisbon, Portugal (2010)
19. R. Moffat, Describing the uncertainties in experimental results. Exp. Therm. Fluid Sci. **1**(1), 3–17 (1988)
20. M. Novara, K. Batenburg, F. Scarano, Motion tracking-enhanced MART for tomographic PIV. Meas. Sci. Technol. **21**(3), 35401 (2010)
21. F. Pereira, M. Gharib, D. Dabiri, D. Modarress, Defocusing digital particle image velocimetry: a 3-component 3-dimensional DPIV measurement technique. Application to bubbly flows. Exp. Fluids **29**(1), S078–S084 (2000)
22. S. Petra, C. Schnörr, A. Schröder, B. Wieneke, Tomographic image reconstruction in experimental fluid dynamics: synopsis and problems, in *Mathematical Modelling of Environmental and Life Sciences Problems* (2007)
23. S. Robinson, Coherent motions in the turbulent boundary layer. Annu. Rev. Fluid Mech. **23**(1), 601–639 (1991)
24. F. Scarano, Tomographic PIV: principles and practice. Meas. Sci. Technol. **24**(1), 012001 (2013)
25. F. Scarano, C. Poelma, Three-dimensional vorticity patterns of cylinder wakes. Exp. Fluids **47**(1), 69–83 (2009)
26. U. Schnars, W. Jüptner, Direct recording of holograms by a CCD target and numerical reconstruction. Appl. Opt. **33**(2), 179–181 (1994)
27. W. Schoppa, F. Hussain, Coherent structure generation in near-wall turbulence. J. Fluid Mech. **453**(1), 57–108 (2002)
28. M. Stanislas, L. Perret, J.-M. Foucaut, Vortical structures in the turbulent boundary layer: a possible route to a universal representation. J. Fluid Mech. **602**, 327–382 (2008)
29. L. Thomas, B. Tremblais, L. David, Optimisation of the volume reconstruction for classical tomo-PIV algorithms (MART, BIMART and SMART): synthetic and experimental studies. Meas. Sci. Technol. **25**(3), 035303 (2014)
30. J. Westerweel, F. Scarano, Universal outlier detection for PIV data. Exp. Fluids **39**(6), 1096–1100 (2005)
31. B. Wieneke, Volume self-calibration for 3D particle image velocimetry. Exp. Fluids **45**(4), 549–556 (2008)
32. C. Willert, Stereoscopic digital particle image velocimetry for application in wind tunnel flows. Meas. Sci. Technol. **8**(12), 1465–1479 (1997)
33. N. Worth, T. Nickels, Acceleration of Tomo-PIV by estimating the initial volume intensity distribution. Exp. Fluids **45**(5), 847–856 (2008)